RSC Advances

PAPER

View Article Online
View Journal | View Issue

Cite this: *RSC Adv.*, 2017, **7**, 52747

3d transition metal doping-induced electronic structures and magnetism in 1T-$HfSe_2$ monolayers

Xu Zhao, * Congxia Yang, Tianxing Wang, Xu Ma, Shuyi Wei and Congxin Xia *

Received 9th October 2017
Accepted 7th November 2017

DOI: 10.1039/c7ra11040e

rsc.li/rsc-advances

By performing first-principles calculations, we explore the structural, electronic and magnetic properties of 3d transition metal (TM) atom-doped 1T-$HfSe_2$ monolayers. The results show that it is energetically favorable and relatively easier to incorporate 3d TM atoms into the $HfSe_2$ under Se-rich experimental conditions. Electronic structures and magnetism can be tuned effectively for V, Cr, Mn, Fe, and Cu doping. We find that the V, Cr, Mn, Fe impurity atoms prefer to stay together in the nearest neighboring (NN) configuration and show ferromagnetism (FM) coupling. Moreover, V-doped $HfSe_2$ shows the characteristics of FM half-metallic properties, and it has lower formation energy. The strong p–d hybridization mechanism is used to explain the magnetism of TM-doped $HfSe_2$ structures. Thus, we can conclude that 3d TM doping can induce the change of electronic structures and magnetism of 1T-$HfSe_2$ monolayers, which is important for applications in semiconductor spintronics.

Introduction

In recent years, two-dimensional (2D) transition metal dichalcogenides (TMDCs), with the chemical formula MX_2 (M = Ti, Zr, Hf, V, Nb, Ta, Cr, Mo, and W, X = S, Se and Te), have been extensively studied due to their highly anisotropic mechanical, distinct electronic, optical, and catalytic properties.[1–22] These materials have superior structure properties of X–M–X-type sandwich structure and much weaker van der Waals between layers, easy cleavage planes parallel to the layers to form low dimensional structures and ease of insertion of atoms or molecules in the interstitial sites between adjacent layers. Layered semiconductor TMDCs have been proven to be important candidates for use as absorber layers for low cost thin film solar cells.[16] This is due to their relatively small band gap (1–2 eV) and large absorption coefficient.[4] Among the TMDCs, MoX_2 and WX_2 have been attracting numerous attentions and have been extensively studied on experimental and theoretical bases. There is a huge number of theoretical works on various properties of the TMDCs layered materials reported to date in the literature. While the electronic and optoelectronic properties of MoX_2 and WX_2 are not good enough, it is necessary to explore the electronic, optical and magnetic properties of other members in the TMDCs family. New findings in transistor and photodetection performance can be anticipated.[13,14] For example, group IVB (Hf and Zr) TMDCs are theoretically predicted to have higher mobility and higher sheet current density than group VIB (Mo and W) TMDs[1,2,5,9,10] and Zhang *et al.* demonstrated that the room-temperature mobility of HfS_2 is much higher than that of MoS_2. The group IVB (Hf and Zr) TMDCs compounds show interesting semiconductor heterojunction properties, half-metallic and optoelectronic properties.[8,13,15,17] HfS_2 and $HfSe_2$ are semiconductors with indirect gaps, while $HfTe_2$ is metallic. Meanwhile, HfX_2 layered semiconductors have been proven to be important candidates for third-generation solar cells with band gaps falling in the range of visible or infrared light regime.[18] Electronic properties of HfX_2 have been investigated by various experimental techniques, including optical absorption, direct and inverse photoemission spectroscopy.[18–22]

Manipulating electronic and magnetic properties of 2D materials by doping TM atoms has raised a lot of attention recently, and a number of experimental and theoretical studies have confirmed that the substitution of TM atoms can induce magnetism in nonmagnetic nanomaterials, such as grapheme, silicene, TMDCs, *etc.*[23–35] Zhou *et al.* confirmed that Mn, Fe, Co, Ni, Cu and Zn substitutions can induce magnetism in the MoS_2 sheet using the first principles calculation.[30] Li *et al.* provided experimentally that Co atoms mainly distribute at the edge of MoS_2 nanosheets, forms hexagonal film, and exhibit half-metallic behavior.[35] The researchers have found that the orientation between the Mn and induced Si moments is ferromagnetic for decoration at the top site and antiferromagnetic for decoration at the hollow site.[25] In addition, quantum anomalous Hall (QAH) effect also has been predicted for magnetically doped thin films of topological insulators,[31] silicene nanoribbons,[32] co-decorated silicene[33] and V-adsorbed germanene and silicone.[34] Meanwhile, inducing spin-polarization in nonmagnetic nanomaterials by doping TM atoms is important because it can lead to scattering[36] and modify the electronic states locally, which is required for

College of Physics and Materials Science, Henan Normal University, Xinxiang, Henan 453007, China. E-mail: zhaoxu@htu.cn; xiacongxin@htu.edu.cn

nanomaterial-based electronics and Kondo physics.[28,37] So, it is expected to understand the electronic and novel magnetic characteristics of TM atoms-doped nanomaterials, and one can see that TM-3d states are expected to exist inside the band gap of the MX_2 sheet, suggesting that the magnetic states of the TM-substituted MX_2 structure can be effectively controlled by engineering the in-gap TM-3d states.

As a candidate material, the 1T-HfX_2 sheet displays interesting semiconductor properties. We have studied the electronic and magnetic properties of TM-doped HfS_2, and find that magnetism is observed for V, Cr, Mn, Fe, Co, and Cu doping.[15] The polarized charges of such a TM-substituted 2D system mainly arise from the localized nonbonding 3d electrons of TM atoms. The results suggest the p–d hybridization mechanism for the magnetism of the TM-doped HfS_2 structures. Depending on the species of TM atoms, the substituted HfS_2 can be a metal, semiconductor or half-metal. TM-doped HfS_2 (TM = V, Fe, Cu) are promising systems to explore two-dimensional diluted magnetic semiconductors. However, the effect of doping transition metal has not been demonstrated for 1T-$HfSe_2$ so far. Therefore, the systematical study of the electronic and novel magnetic characteristics in TM atoms-doped 1T-$HfSe_2$ would be highly desirable. In our present study, we analyze the structural, electronic, and magnetic properties of 1T-$HfSe_2$ doped by the transition metals Sc, Ti, V, Cr, Mn, Fe, Co, Ni, Cu and Zn.

Theoretical models and methods

The first-principles calculations were carried out by using the Vienna *ab initio* simulation package (VASP)[38] based on the density functional theory (DFT) in which projector augmented wave (PAW) method[39] is implemented. During our calculation, the generalized gradient approximation (GGA), electron exchange and correlation, Perdew–Burke–Ernzerhof (PBE) parametrization[40] is used. In all calculations, all structural parameters including the lattice constants (a and c) and the internal coordinate (u) were fully relaxed. An energy cutoff of 500 eV for the plane-wave expansion of the wavefunctions was used. A 5×5 1T-$HfSe_2$ supercell with one (or two) substituted TM atom was used to model the doped $HfSe_2$ structure, which is large enough to avoid interactions of TM atoms between the supercell. Ten different 3d TM atoms were considered to substitute the Hf atom. The Brillouin-zone integrations are performed by using the special k-point sampling of the Monkhorst–Pack scheme. The k-points $9 \times 9 \times 1$ are used for the two-dimensional 1T-$HfSe_2$ supercell. In order to avoid any artificial interaction between neighboring images, the vacuum layer along z-direction is at least 15 Å for the $HfSe_2$ supercell. All the structures are fully relaxed to minimize the total energy of the systems until a precision of 10^{-5} is reached. Both the atomic positions and cell parameters are optimized until the residual forces fall below 0.01 eV $Å^{-1}$.

Results and discussion

$HfSe_2$ adopts the CdI_2 structure (1T structure) with the space group $P\bar{3}m1$ (see Fig. 1), consisting of a layer of Hf atoms sandwiched between two layers of Se atoms. The Hf atom is octahedrally coordinated with the chalcogen atoms. The lattice parameters a and c are optimized in the self-consistent calculation for trigonal crystal structure ($a = 3.74$ Å, $c = 6.14$ Å).[19] The optimized lattice constants are $a = 3.75$ Å, $c = 6.68$ Å, and the Se–Hf bond length ($d = 2.680$ Å) of $HfSe_2$ which is in excellent agreement with experimental measures.

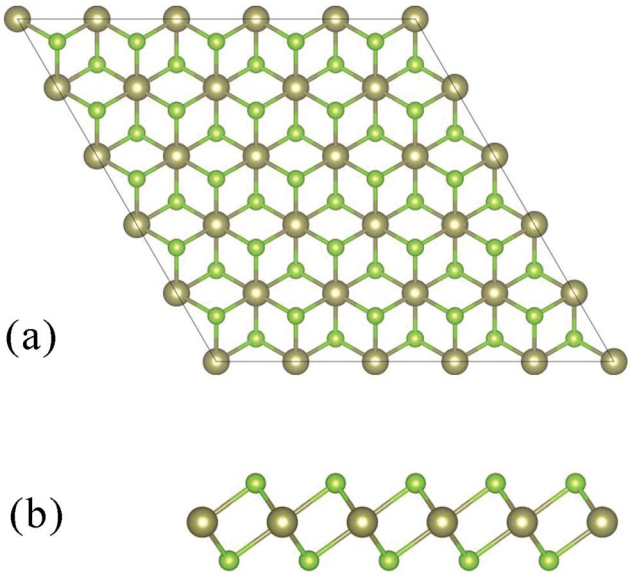

Fig. 1 Schematic structure of 1T-$HfSe_2$ and the top a and side b vies of layered forms are shown. The brown and green balls represent Hf and Se atoms, respectively.

In this work, we investigate firstly the structural and electronic properties of 3d TM-doped 1T-$HfSe_2$ monolayer. The calculated Se–TM bond length, d_{Se-TM}, and magnetic moment, M_{tot} (M_{TM}), and total energy of doped system, E_{tot} and the formation energy in different experimental conditions, E_{form} are listed in Table 1. It can be seen that the d_{Se-TM}, except for d_{Se-Sc} and d_{Se-Zn}, is smaller than 2.680 Å, indicating the covalent-bond

Table 1 The calculated Se–TM binding length, d_{Se-TM}, and magnetic moment, M_{tot} and M_{TM}, and total energy of doped system, E_{tot} and the formation energy in different experimental conditions, E_{form} in TM-doped 1T-$HfSe_2$

System	d_{Se-TM} (Å)	M_{tot} (M_{TM}) (μ_B)	E_{tot} (eV)	E_{form} (eV) Hf-rich	E_{form} (eV) Se-rich
Sc	2.718	0.00	−520.858	0.005	−4.073
Ti	2.600	0.00	−521.363	0.925	−3.153
V	2.578	1.067 (1.378)	−520.770	2.693	−1.385
Cr	2.596	2.034 (2.138)	−521.036	2.96	−1.118
Mn	2.544	2.950 (3.077)	−520.476	2.964	−1.114
Fe	2.520	−1.992 (−1.993)	−518.545	4.302	0.224
Co	2.503	0.00	−517.298	4.323	0.245
Ni	2.489	0.00	−515.743	4.348	0.27
Cu	2.629	1.143 (0.406)	−512.919	5.37	1.292
Zn	2.723	0.00	−511.405	4.425	0.347
Pure	2.680	0.00	−524.486		

interaction between TM and Se atoms is enhanced. As the decrease of atomic size, the d_{Se-TM} decreases from Sc to Ni, except for V, and then increases from Ni to Zn. The shortest d_{Se-TM} of 2.489 Å is found for a Ni impurity, which is similar to TM-doped HfS_2 monolayer.[15] Introduction of magnetism is an exciting research field of nanomaterial, some studies have shown that the polarized charges of such a TM-substituted 2D system mainly arise from the localized nonbonding 3d electrons of TM atoms.[29,33] Our calculations demonstrate that no magnetic moment is observed for Sc, Ti, Co, Ni, Zn substitution case. The magnetic moment is induced for V, Cr, Mn, Fe and Cu doping. The electronic configurations of isolated V, Cr, Mn, Fe and Cu atom are $3d^4 4s^1$, $3d^5 4s^1$, $3d^5 4s^2$, $3d^6 4s^2$, $3d^{10} 4s^1$, respectively. They have 1, 2, 3, 4 and 7 additional valence electrons compared to Hf ($5d^2 6s^2$) atom, which consist with about 1, 2, 3, −2 and 1 μ_B magnetic moments of V-, Cr-, Mn-, Fe- and Cu-doped system. The quantitative analysis of charge distribution and magnetic moment of X-doped 1T-$HfSe_2$ monolayer with closed shall systems (only atoms with obvious magnetic moment) are given in Table 2. From Table 2, we can obtain the similar result that the polarized charges mainly arise from the localized 3d electrons of the TM atom while the contribution of six nearby Se atoms is relatively small.

To probe the stability of the TM-doped 1T-$HfSe_2$, the formation energy E_{form} can be calculated according to the following formula[41,42]

$$E_{form} = E_{(doped)} - E_{(pure)} + n(\mu_{Hf} - \mu_{TM})$$

where $E_{(doped)}$ and $E_{(pure)}$ are the total energies of the 1T-$HfSe_2$ with and without the TM dopants. μ_{Hf} and μ_{TM} are the chemical potential for Hf host and TM dopant atoms, respectively, which depends on the material growth conditions. n is the number of Hf atoms replaced by TM dopants. We use the energy per atom of TM metal as μ_{TM}. The chemical potential μ_{Hf} is defined within a range of values corresponding to Hf-rich or Se-rich growth conditions. For a Hf-rich condition, μ_{Hf} is taken as the energy of isolated Hf atom, while for an Se-rich condition, μ_{Hf} is determined from the difference in energy between a diatomic S_2 molecule and one formula unit of stoichiometric 2D $HfSe_2$. We can see from Table 1 that for the TM-doped 1T-$HfSe_2$, the formation energy is lower under Se-rich conditions, which indicates that it is energetically favorable and relatively easier to incorporate TM atom into 1T-$HfSe_2$ under Se-rich experimental conditions. The smallest E_{form} of −4.073 eV was found for a Sc substitution, the largest E_{form} of 1.292 eV was found for a Cu substitution, which indicates that Sc-doped 1T-$HfSe_2$ is more stable and is a perfect substitution for the Hf atom under Se-rich conditions. Moreover, V-doped $HfSe_2$ has relatively low formation energy in comparison with Cr, Mn, Fe and Cu-doped systems.

The electronic band structures of pristine and one TM-doped $5 \times 5 \times 1$ $HfSe_2$ are given in Fig. 2. Beal *et al.*[43] measured the transmission spectra (0.5–4.5 eV) of single crystals of HfS_2 and $HfSe_2$. Our calculations show that the VBM is located at Γ and CBM at M in agreement with Murray *et al.*[44,45] We give details of electronic structure the doped 1T-$HfSe_2$ systems in Fig. 2. From

Table 2 The charge distribution and magnetic moment of X-doped 1T-$HfSe_2$ monolayer with closed shall systems (only atoms with obvious magnetic moment are given)

	s	p	d	Total charge	Magnetic moment
V-doped system					
V	0.375	0.559	3.225	4.159	1.378
Se48	1.461	2.388	0.030	3.879	−0.025
Se12	1.461	2.375	0.029	3.866	−0.039
Se42	1.461	2.385	0.029	3.876	−0.028
Se50	1.461	2.388	0.030	3.879	−0.025
Se38	1.461	2.375	0.029	3.866	−0.039
Se18	1.461	2.386	0.029	3.876	−0.028
Cr-doped system					
Cr	0.319	0.435	4.202	4.956	2.138
Se48	1.461	2.382	0.029	3.872	−0.034
Se12	1.461	2.383	0.029	3.873	−0.034
Se42	1.461	2.382	0.029	3.872	−0.034
Se50	1.461	2.382	0.029	3.872	−0.034
Se38	1.461	2.383	0.029	3.873	−0.034
Se18	1.461	2.383	0.029	3.873	−0.034
Mn-doped system					
Mn	0.025	0.026	3.053	5.497	3.077
Se48	0.000	−0.040	0.001	3.862	−0.039
Se12	0.000	−0.040	0.001	3.861	−0.039
Se42	0.000	−0.040	0.001	3.862	−0.039
Se50	0.000	−0.040	0.001	3.862	−0.039
Se38	0.000	−0.040	0.001	3.861	−0.039
Se18	0.000	−0.040	0.001	3.862	−0.039
Fe-doped system					
Fe	0.342	0.424	6.261	7.028	−1.993
Se48	1.464	2.365	0.031	3.86	0.028
Se12	1.464	2.357	0.030	3.852	0.020
Se42	1.464	2.365	0.031	3.86	0.028
Se50	1.464	2.365	0.031	3.86	0.028
Se38	1.464	2.357	0.030	3.852	0.020
Se18	1.464	2.365	0.031	3.86	0.028
Cu-doped system					
Cu	0.333	0.301	9.127	9.761	0.406
Se48	1.466	2.355	0.027	3.848	0.127
Se12	1.466	2.355	0.027	3.848	0.133
Se42	1.466	2.353	0.027	3.846	0.125
Se50	1.466	2.355	0.027	3.848	0.127
Se38	1.466	2.355	0.027	3.848	0.133
Se18	1.466	2.353	0.027	3.846	0.125

Fig. 2, we can see that the band gap of pristine 1T-$HfSe_2$ monolayer is 0.590 eV, and some impurity levels emerge within the band gap of the pristine 1T-$HfSe_2$ and these impurity states are mainly from the 3d electrons of TM atoms. For Sc, Cr, Co and Zn doping, the Fermi level moves to the valence band. Among of them, Cr, Fe and Cu-doped systems show magnetic metal properties. Mn-doped system shows magnetic semiconductor property. For Sc, Co, Zn substitutions, the calculated band structures show nonmagnetic metallic properties. And for Ti, Ni substitutions, the band structures show nonmagnetic semiconductor properties. For V-doped $HfSe_2$ shows half metallic properties and can be predicted the good diluted

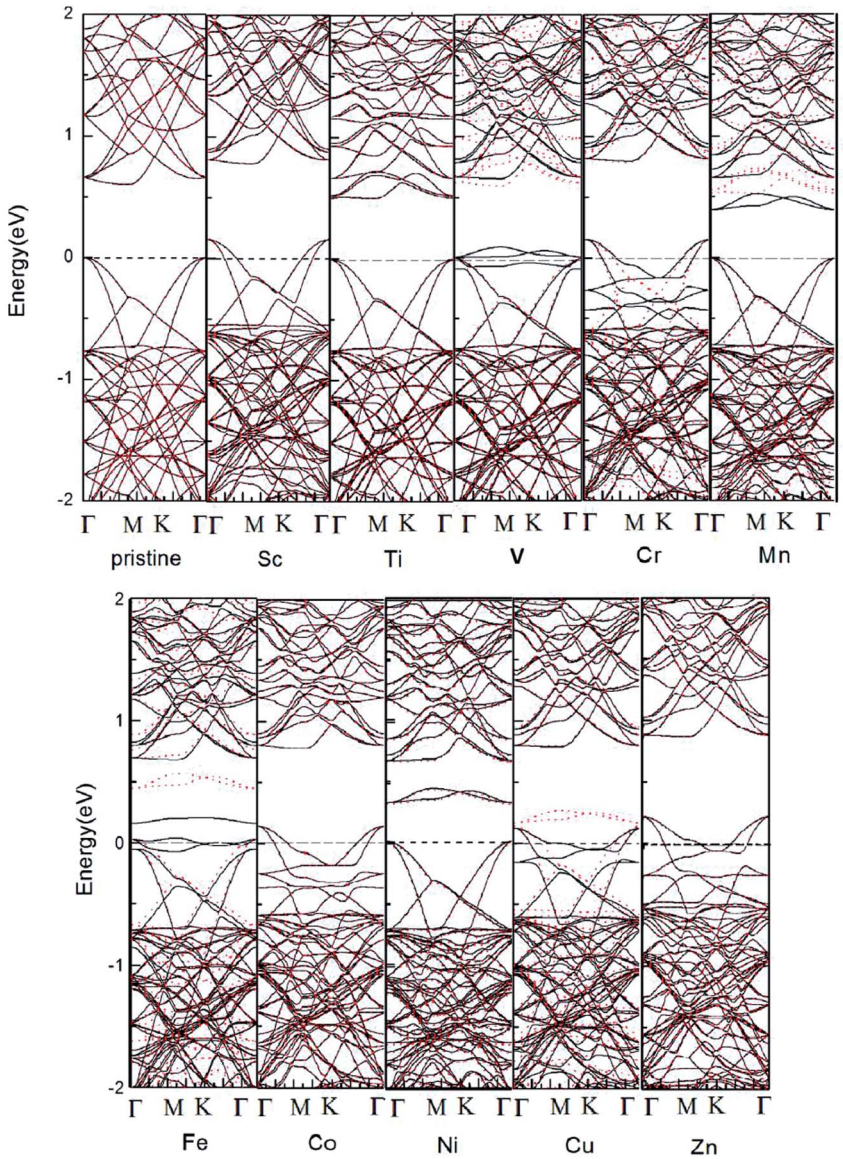

Fig. 2 Band structures of pristine and one TM-doped $5 \times 5 \times 1$ 1T-$HfSe_2$. The black lines and red dot lines represent the spin-up and spin-down components, respectively, where the Fermi level is indicated by the dot line.

magnetic semiconductors, which is suitable for spin injection. The 100% spin polarization near the Fermi level here ensures a high degree of passage of preferred spin, and thus the V-doped system may be possible for spin filter device applications.

In order to understand the magnetic properties in more detail, we investigated the total density of states (TDOS) and the partial density of states (PDOS) for TM-doped 1T-$HfSe_2$ in Fig. 3. From Fig. 3, for the substituted V, Cr, Mn, Fe, and Cu atoms, the spin-up states do not completely match spin-down states, and some sharp spin states of the TM atom emerge near the Fermi level. The sharp features indicate that the polarized electrons are rather local and mainly locate around the TM atom and the neighbor Se atoms. The strong hybridization was found when V, Cr, Mn, Fe, and Cu atoms substituting Hf atom, and mainly from the 3d orbitals of TM and 4p orbitals of Se, which indicated that the substituted TM atom can bond strongly to the Se atom in the 1T-$HfSe_2$ structure, providing a further support of the covalent-bond character. It can also be seen from Fig. 3 that the $d_{x^2-y^2}$ orbital of V significantly overlap with the p_z orbital of Se, the d_{xy} orbital of Fe overlap with the p_y orbital of Se near the Fermi level. For the case of Cr-doped, the impurity states are mainly composed by Cr d_{z^2} orbitals and Se p_y orbitals, and deeply buried in the valence band. By comparison, the impurity states for Mn-doped are close to the conduction band, which indicate be a n-type doping semiconductor.

To visualize the spin distribution of doped 1T-$HfSe_2$ structure, the isosurface spin density is also plotted in Fig. 3, which gives the similar result that the polarized charges mainly arise from the localized 3d electrons of the TM atoms while the contribution of six nearby Se atoms and the interstitial regions is relatively small (except for Cu-doped system). The magnetism for the Cu-doped $HfSe_2$ is somewhat different from the case of

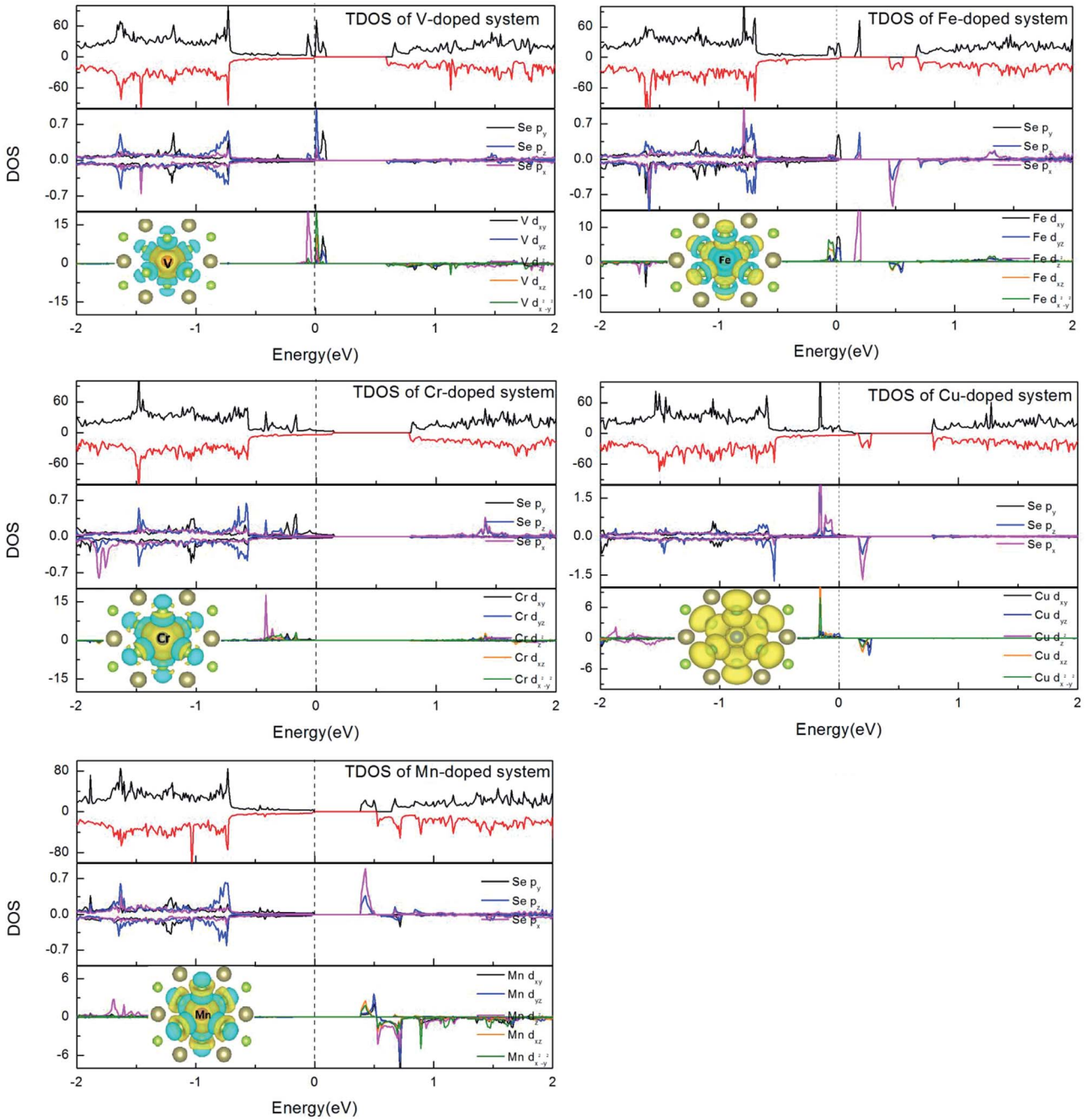

Fig. 3 TDOS of TM-doped 1T-$HfSe_2$ and PDOS of TM dopants and its neighboring Se atoms in TM-doped 5 × 5 × 1 1T-$HfSe_2$. Spin densities of one TM dopants (TM = V, Cr, Mn, Fe and Cu) and its neighboring Se atoms in the TM-doped 5 × 5 × 1 1T-$HfSe_2$. Yellow and aqua isosurfaces represent positive and negative spin densities (+0.001 e $Å^{-3}$), respectively.

other TM atoms. As Cu has filled d shells, a considerable part of the atom magnetization comes from the s and p states (30% for Cu).[29] Moreover, about half of the total magnetization is due to the neighboring six Se atoms. The hybridization between the TM dopant and its neighboring Se atoms results in the splitting of the energy levels near the Fermi energy. These results suggest the p–d hybridization mechanism for the magnetism of the TM-doped $HfSe_2$ structures. For V, Cr, Mn and Fe doping, the spins of the dopants are antiparallel to the induced spins of the nearest six Se atoms, so the total magnetic moment is smaller than the local magnetic moment of the dopants (see Table 1). While for the Cu doping, the induced spins on the nearest Se atoms are all parallel to that of the doped TM, which give rise to the much larger total magnetic moment.

Next, we further calculated two TM atoms replacing two Hf atoms in the 5 × 5 × 1 supercell to investigate the ferromagnetic properties of two TM (V, Cr, Mn, Fe and Cu) doping at 8% impurity concentration. There configurations with different

TM–TM separations were considered: NN configurations in which the two TM atoms are in the nearest neighboring position, the second NN configurations in which the two TM atoms are in the next nearest-neighboring position, and the third NN configuration in which the two TM atoms are in the third nearest-neighboring position. The optimized TM–TM bond length, D_{TM-TM}, and magnetic moment, M_{tot}, and the FM and AFM states energy for the three configurations, E_{FM} and E_{AFM} and the energy differences between the FM and AFM states, E_{FM}–E_{AFM} are listed in Table 3. For V doping, the energy difference between the FM and AFM states are negative for all the three configurations, which indicates the FM states are more favorable energetically. For Cr, Mn and Fe doping, the FM states are more favorable for the NN and 2nd NN configuration, while E_{FM}–E_{AFM} is very small, it is easy to switch the magnetic states to non-magnetic states for the 3rd NN configuration. These results are consistent with the other 2D materials.[23,24] So we predict FM couplings are more favorable for the dopants in NN configurations for Cr, Mn, Fe doping. For the case of Cu doping, FM states appear at 2nd NN configuration, it's interesting that there is no magnetic moment induced to at NN and 3rd NN configuration. From Table 3, we found that the total energy of NN configuration is lowest among of three configurations and the impurity atoms prefer to stay together in the nearest neighboring (NN) configuration.

Fig. 4 gives the total density of states (TDOS) for two TM-doped 1T-$HfSe_2$ at 8% impurity concentration, we see that the impurity states appear within the band gap for all the doped systems and are mainly contributed by the TM 3d states. For the V, Mn doping, the impurity states lie near the conduction band edge, while for Cr, Fe and Cu doping, the impurities states are more close to the valence band edge. Additionally, Cr, Fe and Cu-doped systems still keep magnetic metal properties. Mn-doped system still keeps magnetic semiconductor property. For V-doped $HfSe_2$ keeps half metallic property, these results show that 3d-doping can tune effectively the electronic structures and magnetics properties of 1T-$HfSe_2$ monolayer.

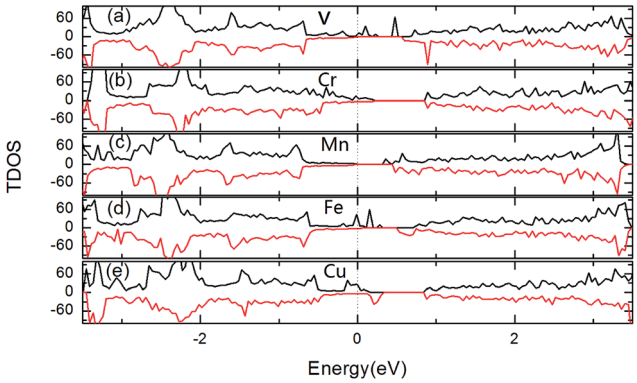

Fig. 4 TDOS of TM-doped 5 × 5 × 1 1T-$HfSe_2$ at 8% impurity concentration.

To understand further the FM properties of two TM atoms doped systems, we give the spin distribution of TM-doped 1T-$HfSe_2$ structure, the isosurface spin density is also plotted in Fig. 5. We find that the polarized charges mainly arise from the localized 3d electrons of the TM atoms (except for Cu-doped system). Moreover, for V, Cr, Mn, Fe doping in the NN configurations, the spins of the two dopants are parallel to each other, which show that the two dopants are FM coupling. While for V, Cr, Mn and Fe doping, the spins of the dopants are antiparallel to the induced spins of the nearest six Se atoms, so the total magnetic moment is smaller than the sum of local magnetic moment of the dopants (see Table 2). For the Cu doping at 2nd NN configuration, the spins of the two Cu atoms are parallel to each other, and the two dopants are FM coupling. The induced spins on the nearest Se atoms are all parallel to that of the doped TM, which give rise to the much larger total magnetic moment. Additionally, the magnetic ordering among the dopants and the nearby host atoms in second and third NN configuration for five doping TM atoms is similar with the situation in the NN configuration.

Table 3 The optimized TM–TM binding length, D_{TM-TM}, and magnetic moment, M_{tot}, and the FM and AFM states energy for the three configurations, E_{FM} and E_{AFM} and the energy differences between the FM and AFM states, E_{FM}–E_{AFM}

System	Configuration	D_{X-X} (Å)	M_{tot} (μ_B)	E_{FM} (eV)	E_{AFM} (eV)	E_{FM}–E_{AFM} (meV)
V-doped	1	3.275	2.110 (V1 = V2 = 1.325)	−517.262	−517.097	−165
	2	6.356	2.284 (V1 = V2 = 1.417)	−517.095	−517.049	−46
	3	7.295	2.256 (V1 = V2 = 1.406)	−517.096	−517.037	−59
Cr-doped	1	3.751	5.332 (Cr1 = Cr2 = 2.900)	−517.535	−517.483	−52
	2	6.495	5.388 (Cr1 = Cr2 = 2.904)	−517.497	−517.485	−12
	3	7.501	5.455 (Cr1 = Cr2 = 2.920)	−517.462	−517.467	0.005
Mn-doped	1	3.735	5.887 (Mn1 = Mn2 = 3.086)	−516.603	−516.573	−30
	2	6.497	5.897 (Mn1 = Mn2 = 3.082)	−516.483	−516.482	−1
	3	7.493	5.902 (Mn1 = Mn2 = 3.080)	−516.432	−516.437	0.005
Fe-doped	1	3.475	−3.937 (Fe1 = Fe2 = −1.958)	−512.882	−512.222	−660
	2	6.435	4.014 (Fe1 = Fe2 = 2.032)	−512.683	−512.676	−7
	3	7.476	4.012 (Fe1 = Fe2 = 2.019)	−512.631	−512.640	0.009
Cu-doped	1	4.394	0.00	−502.406	−502.406	0
	2	6.519	2.335 (Cu1 = Cu2 = 0.335)	−501.308	−501.297	−11
	3	7.558	0.00	−501.400	−501.400	0

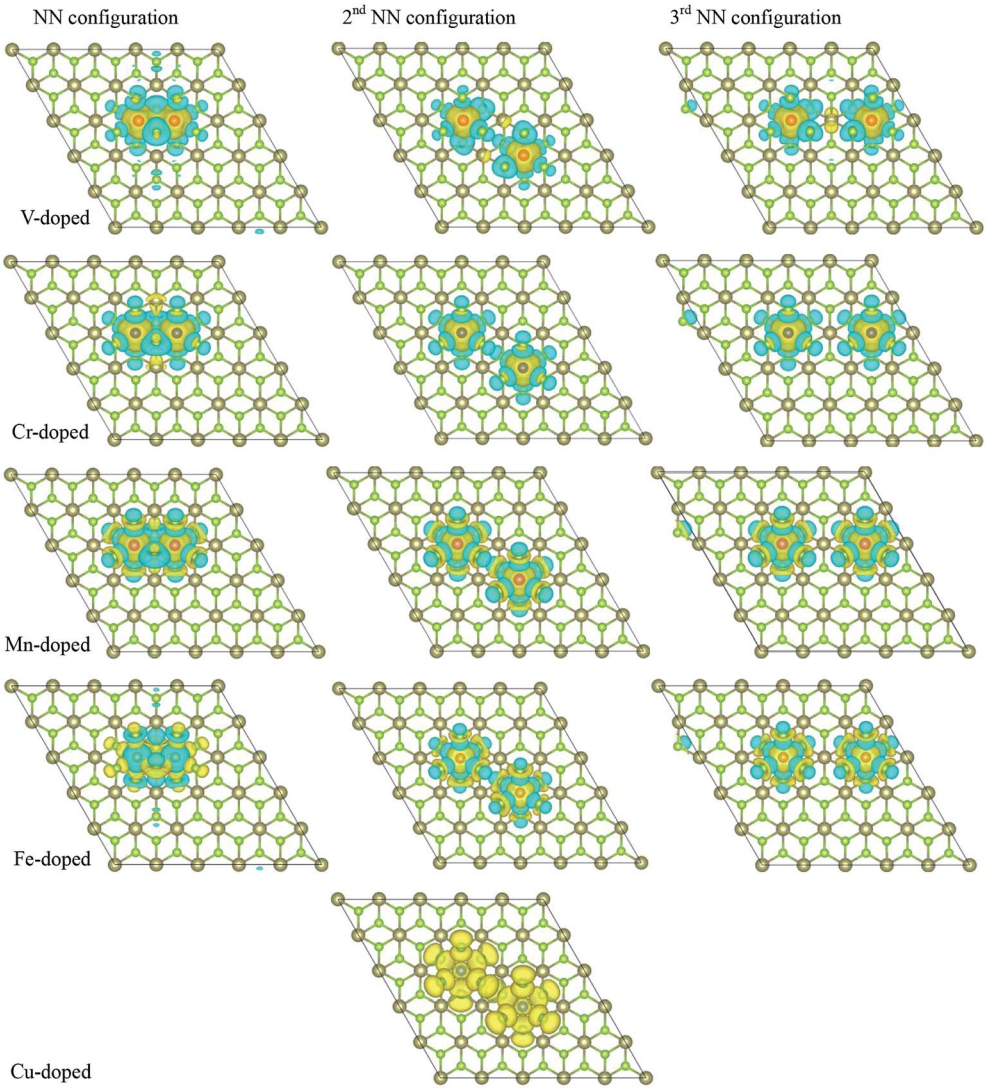

Fig. 5 Spin densities of two TM dopants (TM = V, Cr, Mn, Fe and Cu) and its neighboring Se atoms in the TM-doped $5 \times 5 \times 1$ 1T-$HfSe_2$ of three configurations at 8% impurity concentration. Yellow and aqua isosurfaces represent positive and negative spin densities (+0.001 e $Å^{-3}$), respectively.

Conclusion

In summary, we have investigated the electronic and magnetic properties of TM-doped 1T-$HfSe_2$ using the first-principles methods. Firstly, the formation energy calculations indicate that it is energetically favorable and relatively easier to incorporate 3d TM atom into the $HfSe_2$ under Se-rich experimental conditions. We also find that magnetism is observed for V, Cr, Mn, Fe, and Cu doping. V-doped $HfSe_2$ has relatively low formation energy in comparison with Cr, Mn, Fe and Cu-doped systems. The polarized charges mainly arise from the localized 3d electrons of TM atoms. The strong p–d hybridization mechanism is used to explain the magnetism of the TM-doped $HfSe_2$ structures. Additionally, we have found that the two doped TM atoms prefer to stay in the nearest neighboring positions and couple with each other ferromagnetically. For V, Cr, Mn, and Fe doping, the induced spins on the nearby host atoms are antiparallel to that of the impurities, whereas for Cu doping, they are parallel to that of the dopants. The Mn doping keeps the magnetic semiconductor properties. Cr, Fe and Cu-doped systems still keep magnetic metal properties. Significantly, V doping shows half-metallic properties and is ideal for spin injection, the two V atoms of three configurations are all FM coupling. We believe that these results are helpful on the further study of the property and application of 1T-$HfSe_2$ based diluted magnetic semiconductor.

Conflicts of interest

There are no conflicts to declare.

Acknowledgements

This work is supported by a Grant from the National Natural Science Foundation of China (NSFC) under the Grant No. 11504092, U1304518 and 11674084, and Science and technology

research key project of education department of Henan province (No. 14A140012), and High Performance Computing Center of Henan Normal University.

References

1 J. Kang, S. Tongay, J. Zhou, J. Li and J. Wu, *Appl. Phys. Lett.*, 2013, **102**, 012111.
2 W. Zhang, Z. Huang, W. Zhang and Y. Li, *Nano Res.*, 2014, **7**, 1731–1737.
3 A. Klein, S. Tiefenbacher, V. Eyert, C. Pettenkofer and W. Jaegermann, *Phys. Rev. B: Condens. Matter Mater. Phys.*, 2001, **64**, 205416.
4 P. P. Hankare, A. H. Manikshete, D. J. Sathe, P. A. Chate, A. A. Patil and K. M. Garadkar, *J. Alloys Compd.*, 2009, **479**, 657–660.
5 L. Li, X. Fang, T. Zhai, M. Liao, U. K. Gautam, X. Wu, Y. Koide, Y. Bando and D. Golberg, *Adv. Mater.*, 2010, **22**, 4151–4156.
6 S. Tongay, J. Zhou, C. Ataca, K. Lo, T. S. Matthews, J. Li, J. C. Grossman and J. Wu, *Nano Lett.*, 2012, **12**, 5576–5580.
7 P. Lu, X. Wu, W. Guo and X. C. Zeng, *Phys. Chem. Chem. Phys.*, 2012, **14**, 13035–13040.
8 X. Zhao, T. Wang, X. Xia, X. Dai, S. Wei and L. Yang, *J. Alloys Compd.*, 2017, **698**, 611–616.
9 H. Jiang, *J. Phys. Chem. C*, 2012, **116**, 7664–7671.
10 G. Fiori, F. Bonaccorso, G. Iannaccone, T. Palacios, D. Neumaier, A. Seabaugh, S. K. Banerjee and L. Colombo, *Nat. Nanotechnol.*, 2014, **14**(9), 768–779.
11 H. Jiang, *J. Chem. Phys.*, 2011, **134**, 204705.
12 Y. Feldman, E. Wasserman, D. J. Srolovitz and R. Tenne, *Science*, 1995, **267**, 222–225.
13 X. Zhao, C. Xia, T. Wang, X. Dai and L. Yang, *J. Alloys Compd.*, 2016, **689**, 302–306.
14 M. Zhong, L. Huang, H. X. Deng, X. Wang, B. Li, Z. Wei and J. Li, *J. Mater. Chem. C*, 2016, **4**, 6492–6499.
15 X. Zhao, T. Wang, G. Wang, X. Dai, C. Xia and L. Yang, *Appl. Surf. Sci.*, 2016, **383**, 151–158.
16 E. Gourmelon, O. Lignier, H. Hadouda, G. Couturier, J. C. Bernède, J. Tedd, J. Pouzet and J. Salardenne, *Sol. Energy Mater. Sol. Cells*, 1997, **46**, 115–121.
17 J. A. Wilson and A. D. Yoffe, *Adv. Phys.*, 1969, **18**, 193–335.
18 M. Moustafa, T. Zandt, C. Janowitz and R. Manzke, *Phys. Rev. B: Condens. Matter Mater. Phys.*, 2009, **80**, 035206.
19 D. L. Greenaway and R. Nitsche, *J. Phys. Chem. Solids*, 1965, **26**, 1445–1458.
20 K. Terashima and I. Imai, *Solid State Commun.*, 1987, **63**, 315–318.
21 S. C. Bayliss and W. Y. Liang, *J. Phys. C: Solid State Phys.*, 1982, **15**, 1283–1296.
22 G. Jakovidis, J. D. Riley, J. Liesegang and R. C. G. Leckey, *J. Electron. Spectrosc. Relat. Phenom.*, 1987, **42**, 275–279.
23 H. J. Monkhorst and J. D. Pack, *Phys. Rev. B: Solid State*, 1976, **13**, 5188–5192.
24 X. L. Fan, Y. R. An and W. J. Guo, *Nanoscale Res. Lett.*, 2016, **11**, 154.
25 T. P. Kaloni, S. Gangopadhyay, N. Singh, B. Jones and U. Schwingenschlögl, *Phys. Rev. B: Condens. Matter Mater. Phys.*, 2013, **88**, 235418.
26 Y. C. Cheng, Z. Y. Zhu, W. B. Mi, Z. B. Guo and U. Schwingenschlögl, *Phys. Rev. B*, 2013, **87**, 100401.
27 Q. Yue, S. Chang, S. Qin and J. Li, *Phys. Lett. A*, 2013, **377**, 1362–1367.
28 T. P. Kaloni, M. U. Kahaly and U. Schwingenschlögl, *J. Mater. Chem.*, 2001, **21**, 18681.
29 A. V. Krasheninnikov, P. O. Lehtinen, A. S. Foster, P. Pyykkö and R. M. Nieminen, *Phys. Rev. Lett.*, 2009, **102**, 126807.
30 Y. Zhou, Q. Su, Z. Wang, H. Deng and X. Zu, *Phys. Chem. Chem. Phys.*, 2013, **15**, 18464–18470.
31 R. Yu, W. Zhang, H. J. Zhang, S. C. Zhang, X. Dai and Z. Fang, *Science*, 2010, **329**, 61–64.
32 M. Ezawa, *Phys. Rev. Lett.*, 2012, **109**, 055502.
33 T. P. Kaloni, N. Singh and U. Schwingenschlögl, *Phys. Rev. B: Condens. Matter Mater. Phys.*, 2014, **89**, 035409.
34 T. P. Kaloni, *J. Phys. Chem. C*, 2014, **118**, 25200–25208.
35 B. Li, L. Huang, M. Zhong, N. Huo, Y. Li, S. Yang, C. Fan, J. Yang, W. Hu, Z. Wei and J. Li, *ACS Nano*, 2015, **9**, 1257–1262.
36 M. I. Katsnelson, F. Guinea and A. K. Geim, *Phys. Rev. B: Condens. Matter Mater. Phys.*, 2007, **79**, 195426.
37 M. Hentschel and F. Guinea, *Phys. Rev. B: Condens. Matter Mater. Phys.*, 2007, **76**, 115407.
38 G. Kresse and J. Furthmüller, *Phys. Rev. B: Condens. Matter Mater. Phys.*, 1996, **54**, 11169–11186.
39 P. E. Blochl, *Phys. Rev. B: Condens. Matter Mater. Phys.*, 1994, **50**, 17953–17979.
40 J. P. Perdew, K. Burke and M. Ernzerhof, *Phys. Rev. Lett.*, 1996, **77**, 3865–3868.
41 C. Xia, Y. Peng, H. Zhang, T. Wang, S. Wei and Y. Jia, *Phys. Chem. Chem. Phys.*, 2014, **16**, 19674–19680.
42 Y. Peng, C. Xia, H. Zhang, T. Wang, S. Wei and Y. Jia, *Phys. Chem. Chem. Phys.*, 2014, **16**, 18799–18804.
43 A. R. Beal, J. C. Knights and W. Y. Liang, *J. Phys. C: Solid State Phys.*, 1972, **5**, 3531–3539.
44 R. B. Murray, R. A. Bromley and A. D. Yoffe, *J. Phys. C: Solid State Phys.*, 1972, **5**, 746–758.
45 A. Hussain Reshak and S. Auluck, *Phys. B*, 2005, **363**, 25–31.

